Robotica (2023), page 1-21 doi:10.1017/xxxxx

CAMBRIDGE UNIVERSITY PRESS

RESEARCH ARTICLE

Design and Control of a Compliant Robotic Actuator with Parallel Spring-Damping Transmission

Peikang Yuan[1], Jianbin Liu[1], David T Branson[2], Zhibin Song[1], Shuai Wu[3], Jian S. Dai[1,4] and Rongjie Kang*[1]

[1]Key Laboratory of Mechanism Theory and Equipment Design of Ministry of Education School of Mechanical Engineering, Tianjin University, Tianjin 300072, China.

[2]Advanced Manufacturing Technology Research Group, Faculty of Engineering, University of Nottingham, Nottingham NG7 2RD, UK.

[3]Research Institute for Frontier Science, Beihang University, Beijing 100191, China

[4]Shenzhen Key Laboratory of Intelligent Robotics and Flexible Manufacturing Systems, Southern University of Science and Technology, Shenzhen 518055, China

*Corresponding author. E-mail: rjkang@tju.edu.cn

Keywords: compliant actuator, variable damping, force control, position control.

Abstract

Physically compliant actuator brings significant benefits to robots in terms of environmental adaptability, human-robot interaction and energy efficiency as the introduction of the inherent compliance. However, this inherent compliance also limits the force and position control performance of the actuator system due to the induced oscillations and decreased mechanical bandwidth. To solve this problem, we firstly investigate the dynamic effects of implementing variable physical damping into a compliant actuator. Following this, we propose a structural scheme that integrates a variable damping element in parallel to a conventional Series Elastic Actuator (SEA). A damping regulation algorithm is then developed for the Parallel Spring-Damping Actuator (PSDA) to tune the dynamic performance of the system while remaining sufficient compliance. Experimental results show that the PSDA offers better stability and dynamic capability in the force and position control by generating appropriate damping levels.

1. Introduction

Robots have been increasingly used in applications requiring physical interactions with environments or human beings, where the adaptability and safety of the robotic actuators become priority. This is usually achieved by introducing compliance to the robotic [1]actuators. Traditional rigid actuators can obtain compliance by properly using impedance control algorithms[2]. However, this active control-based method requires sensors and controllers to have fast response, which are difficult to meet for in many cases [3].

Introducing physical compliance (elastic or soft materials) in robot systems plays a pivotal role in solving the interaction problem[4-6]. Compared with rigid ones, physically compliant actuators, for example, the Series Elastic Actuator (SEA) [7-10], utilize elastic element as the transmission component, which provides passive compliance to the robotic systems. Even under sudden collisions, the passive filtering of the impact through the elastic element is faster and more reliable than that achieved by an active impedance control algorithm[3]. Besides, the deformation of the embedded elastic elements is measurable, so the force control can be converted to the position control [11], to

reduce the control difficulty and improve the stability. The elastic element can also absorb and release shock energy with proper control method, improving the energy efficiency of the actuator[12-14].

Despite the above-mentioned advantages of SEA, they do have some drawbacks due to the introduction of elastic elements, including (1) the reduced bandwidth will limit the dynamic performance of force and position control, (2) the system is susceptible to oscillations. If the actuator is fast enough, these oscillations may be suppressed by applying active damping control, however, this highly dynamic process would require a substantial amount of energy input [3].

There have been a number of works on improving the bandwidth of physically compliant actuators. When Pratt proposed the SEA [7] for the first time, he also proposed a method using an SEA and a rigid actuator connected in parallel to drive a joint. The SEA is used in low-frequency tasks, while the rigid one used for high-frequency operations [15, 16]. This method can only switch between either low or high bandwidth. Subsequently, Variable Stiffness Actuator (VSA) was proposed[17-20]. The stiffness of the VSA can be adjusted continuously according to the control demand. Although VSA can improve the bandwidth, if necessary, it still has the problem of system oscillation. In addition, many VSAs, especially those with antagonistic setups [21-23], need to consume a lot of energy to regulate and maintain the stiffness.

To solve the oscillation problem, Hurst implemented an additional damper to the SEA to suppress the oscillations on the output link[24]. However, it was a constant damper that may cause a force spike at the beginning of a collision if the level of the damping value is set too high. Therefore, the demand for tunable damper is proposed. The Variable Damping Actuators (VDAs)[25, 26] can change its physical damping to suppress the system oscillation. Laffranchi utilized a piezoelectric damper[26], which essentially operates as a friction damper by actively controlling friction force to mimic viscous damping effect. It needs to apply a normal force to the friction surfaces to maintain the damping effect, which is energy consuming. To the best of our knowledge, so far, the existing VSA or VDA are not able to solve the dynamic and energy issues at the same time.

Inspired by SEA, Chee-Meng proposed a Series-Damper-Actuator (SDA) for force control in[27]. Unlike the VDA mentioned previously, the SDA purely uses a fluid dynamic damper as a transmission element without any elastic element. Therefore, the SDA has a larger output force bandwidth than SEA, and avoids the problem of system oscillation. However, the removal of elastic element makes it impossible to store and re-use the energy. Besides, SDA cannot transfer torque when it is stationary or moving at low speed.

Considering the pros and cons of previous SEA and SDA, the purpose of this paper is to design a physically compliant actuator capable of damping adjustment with low energy consumption, while improving the dynamic performance (e.g. less oscillations, fast response) of the actuator. This work bridges the gap between dynamics and efficiency for a robotic actuator, which was not reported in the previous works. To achieve these aims, we develop a Parallel Spring-Damping Actuator (PSDA). The transmission mechanism of the PSDA is composed of an elastic element and a variable damper arranged in parallel. The stiffness of the elastic element is constant, while the damping level of the damper can be adjusted actively. The reason for using variable damping is that it can effectively suppress the oscillation caused by the elastic element. The characteristics of the PSDA can be more like an SDA having a high bandwidth if the damping is increased. On the other hand, the damping in the PSDA can also be adjusted to a low level, like an SEA, to store as much impact energy as possible in the elastic element. In other words, the PSDA can run in an SDA or SEA mode according to the working condition, combining the advantages of both. The main contributions of the work include:

(1) Structure design: We developed a variable damping mechanism by implementing a fluidic orifice with tunable area. Once the area of the orifice is set, no more energy input is required to maintain the damping, resulting in high energy efficiency. Moreover, when the orifice is completely closed, the incompressibility of the fluid makes the damper equivalent to a rigid connection. This means that the system can be regarded as a rigid actuator, achieving high precision and dynamics. The variable damping mechanism is embedded into the shaft of the actuator, resulting in a compact structure.

(2) Control strategy: Based on the structure of the actuator, our paper proposed a new variable

damping control algorithm. This algorithm can predict the changes in the reference signals (desired signals) and adjust the damping level accordingly. Through simulations and experiments, we have demonstrated that the presented algorithm is effective in suppressing oscillations caused by the elastic elements, while improving the dynamic response of the actuator in both force and position control scenarios.

The rest of the paper is organized as follows. Sections 2 studies the effects of embedding a parallel physical damping in a compliant actuator for the force and position control. Section 3 presents the design of the variable damping mechanism and its implementation into a PSDA whose dynamic model is explained in Section 4. The control scheme for the PSDA is analyzed in Section 5 and experimental results are presented in Section 6.

2. Analysis of the Parallel Damping

As mentioned in Section 1, we proposed a PSDA scheme composed of parallelly arranged elastic element and variable damper to the transmission between the motor and output link. In this section, we analyze the effects of the variable damping on the force control, position control, and system compliance.

2.1. Force Control

In many previous works[28-30], the force control of SEA was described by a one-mass model, as shown in Fig.1(a), in which the output link of the SEA is considered to be fixed with the environment. Therefore, the interaction occurs between the motor and the environment. We adopt this one-mass modelling method by adding a parallel variable damping to the SEA, as shown in Fig.1(b).

According to the dynamic relationship shown in Fig. 1(b), the transfer function of the PSDA from the motor force τ_m to the interaction force τ_o can be written as

$$F_f(s) = \frac{\tau_o(s)}{\tau_m(s)} = \frac{D_t s + K}{J_m s^2 + D_t s + K} \tag{1}$$

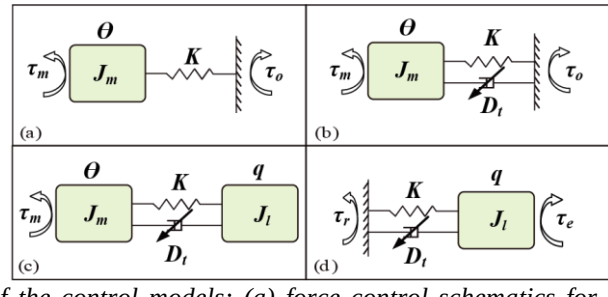

Figure 1. *Diagram of the control models: (a) force control schematics for SEA, (b) force control schematics for PSDA, (C) position control schematics for PSDA and (d) Impact model of the PSDA, where τ_m is the motor torque, τ_o is the interaction force,J_m is the inertia of the motor, K is the spring constant, D_t is the damping coefficient, θ is the position of the motor, and q is the position of the output link.*

According to Eq. (1), it can be seen that the force control system is composed of a second-order oscillation part (the denominator part) and a differential part (the numerator part). The system oscillation is mainly determined by the damping ratio of the second-order oscillation part, which is

$$\xi = \frac{D_t}{2\sqrt{J_m K}} \tag{2}$$

To suppress the oscillation, we can increase the damping ratio by increasing the physical damping D_t. However, increasing the damping ratio usually means a reduction of the dynamic response. Note that, the system also contains a differential part that can improve the dynamic response of the system with the increase of the damping D_t [31]. Then, it is hard to say whether increasing the damping will improve or reduce the dynamic response of the system intuitively. In order to investigate the effect of the parallel damping on the force control system, we plot the bode diagrams of the transfer function $F_f(s)$ with different damping D_t. As shown in Fig.2, the PSDA can be considered as a SEA when D_t= 0, and there is a sharp magnitude peak at the resonance point, which means that SEA is an underdamped system and prone to oscillation. By increasing the value of D_t, a reduction of the magnitude peak at resonance point is evident. And the bandwidth of the PSDA system can be greatly increased accordingly. Therefore, for the force control, the parallel damping D_t not only suppresses the system oscillations, but also improves the dynamic response of the system.

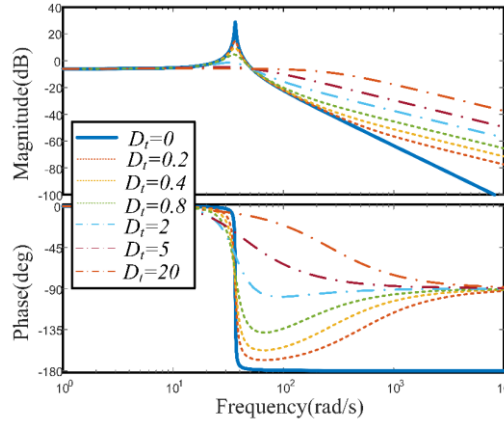

Figure 2. *Bode plot of the transfer function of the force control model, $F_f(s)$, considering different damping levels $D_t \in [0,20]$ Nms/rad. By increasing the value of D_t, a reduction of the magnitude peak at the resonance point is observed. And the bandwidth of the PSDA system can be greatly increased accordingly. The other parameters, K=50 Nm/rad, J_m=0.1 kg m2, are used according to literature[32, 33].*

2.2. Position Control

For position control, the output link is the controlled plant, thus, we have to take it into account in the model. As shown in Fig.1(c), the dynamics of the position control system can be written as

$$\begin{cases} \tau_m - D_t(\dot{\theta} - \dot{q}) - K(\theta - q) = J_m \ddot{\theta} \\ D_t(\dot{\theta} - \dot{q}) + K(\theta - q) = J_l \ddot{q} \end{cases} \tag{3}$$

According to Eq. (3), the transfer function of the PSDA from the motor torque τ_m to the output link position q is

$$F_p(s) = \frac{q(s)}{\tau_m(s)} = \frac{D_t s + K}{[J_m s^2 + D_t s + K][(J_l s^2 + D_t s + K)] - (D_t s + K)^2} \tag{4}$$

where J_l is the inertia of the output link and q is the position of the output link. It can be seen that the

position control system is a four-order system composed of two second-order oscillation part and a differential part, and the damping D_t affects every part. A Bode plot of the system with different damping level D_t is shown in Fig.3. The PSDA can be considered as an SEA when D_t = 0 with a sharp magnitude peak at the resonance point. Similar to the case of the force control, the magnitude peak can be reduced by increasing the damping D_t, but the increase of bandwidth is not as significant as that in the force control. This is because the damping force is directly involved in the output force in force control. However, in position control, the damper functions as a transmission component to affect the output velocity and position. To tackle this issue, we present a design that enables the actuator to switch to a rigid state, thereby enhancing its stiffness and improving the dynamics of the position control system. Detailed information regarding this specific design can be found in Section 3.2.

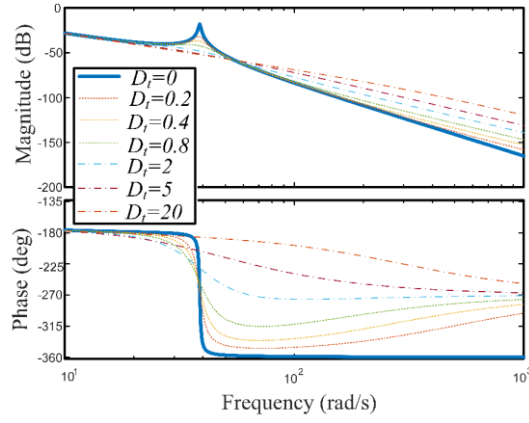

Figure 3*. Bode plot of the PSDA considering different damping D_t levels from 0 to 20Nms/rad. By increasing the value of D_t, a reduction of the magnitude peak at the resonance point is observed.*

2.3. System Compliance

According to the above analysis, it can be seen that the performance of both force and position control can be improved by increasing the value of the parallel damping D_t. However, if we simply set the damping to a high level, it will reduce the compliance of the actuator. There will be a reaction force when the output link of the actuator is subjected to an impact force.

As shown Fig.1(d), an impact model for the system can be described as

$$J_l\ddot{q}+D_t\dot{q}+Kq=\tau_e \tag{5}$$

where τ_e is the impact torque acting on the output link. Thus, a reaction torque τ_r generated by the elastic and damping elements is

$$\tau_r = D_t\dot{q}+Kq \tag{6}$$

For the PSDA, the stiffness K is constant, and we are more interested in how the damping D_t affects the reaction torque, which is a representation of the compliance. In Fig.4(a), we use a square wave pulse signal to simulate the impact torque, and the reaction torque is extremely sharp at high damping level (D_t=10). However, the reaction torque exhibits vibration like a sin-wave at a low damping level (D_t=0.1). This proves that the use of high damping will reduce the compliance of the system.

We have also analyzed the energy conversion process of the system during the impact. The impact energy stored and reused by the elastic element is $E=Kq^2/2$ for a physically compliant actuator. We

plot the change of elastic potential energy during the impact in Fig.4(b). It shows that only a small part of the impact energy can be converted into elastic potential energy when the damping is at a high level. In this case, the effect of the elastic component is very limited as most of the energy is consumed by the high damping. In other words, the system is lacking in compliance.

According to the above analysis, over damping may reduce the compliance of the system and therefore affects the safety. However, an under damping system cannot guarantee the dynamic performance of force and position control. Note that, the criterion for over or under damping are not unique in different situations, which motivates us to develop the PSDA with variable damping.

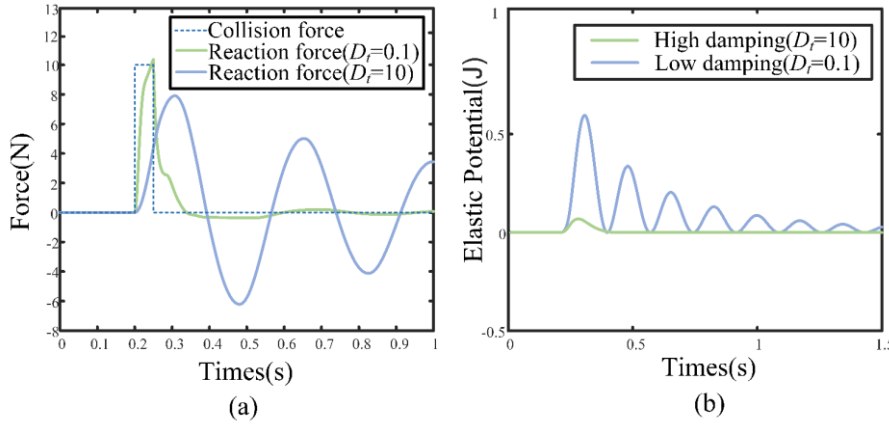

Figure 4. *impact analysis with different damping (a) response of reaction force (b) energy change in the elastic component. The peak of the reaction torque is significant at a high damping level (D_t=10), and minimal impact energy can be converted to elastic potential energy at this level of damping.*

3. Design and Implementation of PSDA

In this section, we present the mechanical design of the PSDA considering the following design requirements. Firstly, the range of variable damping should be as large as possible. Secondly, the energy used to maintain the damping should be as little as possible. Thirdly, the size of the actuator should be compact.

3.1. The Variable Damping Mechanism

At present, there have been several methods used to achieve variable damping. Magnetorheological and electrorheological fluid-based dampers[34-36] were adopted in automotive and civil engineering applications. However, they need to continuously apply magnetic field or current to maintain the physical damping, which will consume a lot of energy. Moreover, they are usually too bulky for robotic systems. Friction-based dampers[26] needs to apply normal force on the friction surface all the time, which is not energy-efficient either. Besides, the abrasion of the friction surface may affect the lifetime of the actuator system. The fluid dynamics-based dampers can tune its physical damping by using the orifice effect [3]. Once the effective area of the orifice is settled, the damping will be maintained at a certain level without further energy input. However, traditional fluid dynamics dampers were not compact enough for robotic applications. In this work, we design a compact damper based on orifice effect that can be integrated to a robotic actuator to provide tunable physical damping.

As shown in Fig.5, the proposed variable damper is composed of a rotating piston and a hydraulic cylinder. There are two baffles fixed to the inner surface of the hydraulic cylinder, and the rotating

piston is assembled between the two baffles. Thus, the hydraulic cylinder is divided into four damping chambers (A1, A2, A3, A4) that are filled with damping medium (hydraulic oil in our case). Two orifices on the rotating piston are used to connect chambers A1 and A2, A3 and A4. If the rotating piston has relative rotation to the hydraulic cylinder, the hydraulic oil will flow from the chambers of reduced volume to that of the increased volume. Due to the orifice effect, there will be a pressure difference between the two sides of the rotating piston and therefore generate the damping torque. We can change the damping torque by using a flap to adjust the effective area of the orifice. Once the position of the flap is set, the physical damping can be maintained without any further energy consumption. To ensure the compactness of the actuator, the piston is connected to the motor shaft and the cylinder is used as the output link of the actuator. The relative motion between the piston and cylinder can be eliminated by closing the orifice, in this case, the actuator can be considered as a rigid actuator, which is good for position control. Therefore, the variable damper allows the actuator to operate in two states: (1) compliant state and (2) rigid state. The structure of the whole actuator system will be detailed in Section 3.2.

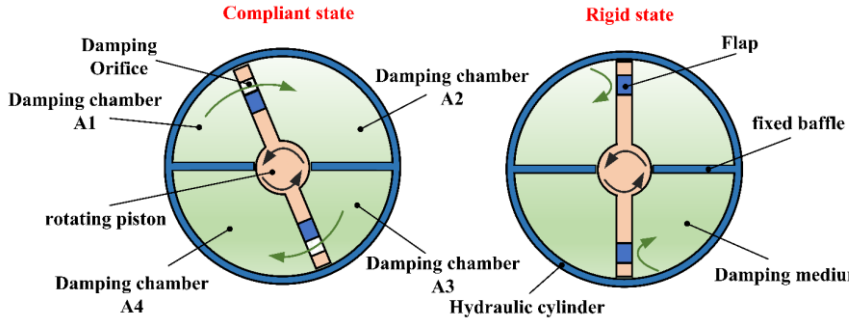

Figure 5. *Conceptual schematic of the orifice-based damper*

3.2. Mechanical Design of the PSDA

Fig.6(a) shows the transmission unit of the PSDA. It is composed of a spring part and a variable damper part, both of which are mounted on the input link of the transmission unit. The spring part has a typical SEA structure that is coupled with the output link of the transmission unit with six compression springs in three groups [37]. The variable damper part utilizes a hydraulic rotating piston and cylinder to transmit the torque from the input link (the rotating piston) to the output link (the rotating cylinder), as mentioned in Section 3.1. The inner space of the hydraulic cylinder is divided into four damping chambers by the rotating piston. There are two damping orifices on the rotating piston, and the hydraulic oil can only flow between the chambers through the damping orifices. Two flaps are installed with the orifices and driven by the linear piston through a T-shaped internal pipe to control the area of the orifices. A linear motor M2 is connected to the linear piston to tune the damping.

The mechanical structure of the PSDA prototype is shown in the Fig.6(b). The servo torque motor M1 equipped with a harmonic drive gearbox is connected to the input link of the transmission unit, providing the main rotating movement of the PSDA. The linear motor M2 embedded in the internal link of the transmission unit is used to tune the damping by changing the area of the orifices. A torque sensor and a 22-bit absolute encoder are mounted on the output link of the PSDA.

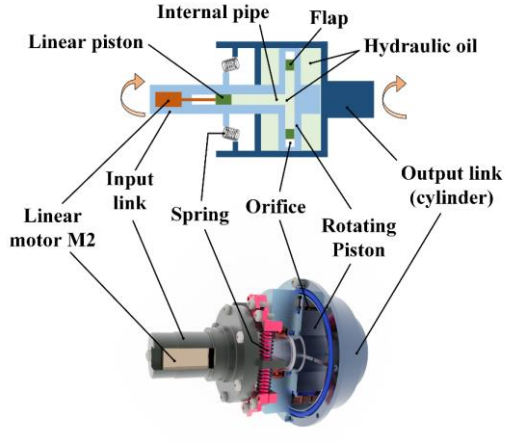

(a)

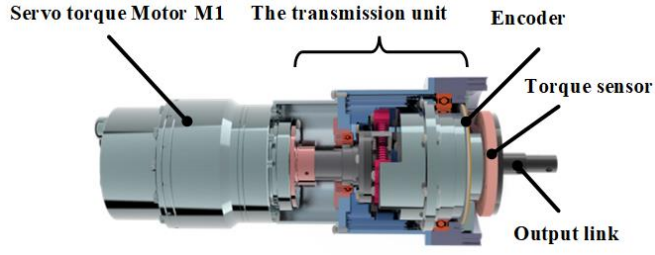

(b)

Figure 6. *Structure of the PSDA (a) The spring-damping parallel transmission unit, (b) the PSDA prototype*

4. Mathematical Model

This section introduces the modeling of the PSDA prototype, including the mathematical model of the variable damper, and the dynamic models for the force and position control, respectively.

4.1. Model of the Variable Damper

Figure 7 shows the geometrics of the variable damping mechanism, and the corresponding parameters are listed in Table I. The flow rate l_q going through the orifice can be calculated as

$$l_q = C_q A_0 \sqrt{2 p/\rho} \tag{7}$$

where C_q is the flow coefficient, $A_0 = \triangle x_1 . y$ is the effective area of the damping orifice, $\triangle p$ is the pressure difference, and $\rho$is the density of the hydraulic oil. On the other hand, the flow rate l_q can also be calculated according to the volume change of the damping chambers swept by the rotating piston that is

$$l_q = h(R^2 - r^2)\omega \tag{8}$$

where ω is the relative rotating speed between the rotating piston and the cylinder. Substituting Eq. (8) to Eq. (7), we can obtain the pressure difference $\triangle p$ as

$$\Delta p = \frac{h^2(R^2 - r^2)^2 \rho}{2C_q{}^2 A_0{}^2} \omega^2 \tag{9}$$

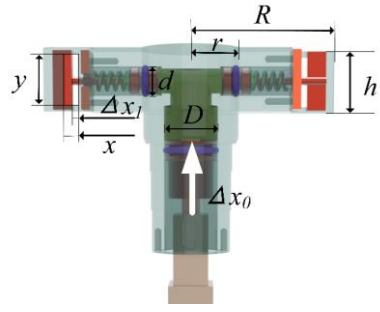

Figure 7. *Geometrics of the variable damping mechanism*

The damping torque τ_D can then be calculated as

$$\tau_D = 2\int_r^R \Delta phxdx = \frac{h^2(R^2 - r^2)^2 \rho}{2C_q{}^2 A_0{}^2} \omega^2 = D_t \omega^2 \tag{10}$$

So, the damping coefficient D_t is

$$D_t = \frac{h^2(R^2 - r^2)^2 \rho}{2C_q{}^2 A_0{}^2} \tag{11}$$

According to Eq. (10), the damping torque τ_D is proportional to the square of the rotating speed ω which means that the proposed damper is nonlinear. Equation (11) shows that the damping coefficient D_t is related to many geometric parameters, among which the effective area A_0 is variable. As mentioned in section 3.2, the effective area A_0 can be adjusted by the linear motor M2 through the T-shaped hydraulic pipe.

TABLE I

The Parameters in the Variable Damping Model

Parameter	Description	Value
$\boldsymbol{R}$	The outer radius of the linear piston	35mm
$\boldsymbol{r}$	The inner radius of the linear piston	125mm
$\boldsymbol{h}$	height of the piston	15mm
$\boldsymbol{y}$	Height of the damping orifices	12mm
$\boldsymbol{d}$	Diameter of linear piston(L2&L3)	7mm
$\boldsymbol{D}$	Diameter of linear piston(L1)	13mm
$\triangle \boldsymbol{x_0}$	Elongation of the Linear motor M2	0~4mm
$\triangle \boldsymbol{x_1}$	Displacement of flap	0~10mm

4.2. Model of the PSDA

The PSDA has two operating modes: force control and position control. In the different modes the PSDA has different dynamics models.

In the force control mode, the PSDA generates an interactive force by considering the output link is fixed to the environment, as mentioned in Section 2.1 and Fig.8 (a). So, the dynamical model can be described as

$$\tau_m - D_t(\Delta x_0)\dot{\theta}^2 \operatorname{sgn}(\dot{\theta}) - D_m\dot{\theta} - K\theta = J_m\ddot{\theta} \tag{12}$$

where $D_t(\Delta x_0)$ is the damping coefficient of the variable damper that can be tuned by the displacement of the linear motor M2, Δx_0. The PSDA transmits the torque to the environment by means of the parallel spring-damping mechanism, so the sum of the spring and the damping torque is the total output torque that can be described as

$$\tau_o = D_t(\Delta x_0)\dot{\theta}^2 \operatorname{sgn}(\dot{\theta}) + K\theta \tag{13}$$

In the position control mode, the position of the output link is the controlled plant as mentioned in section 2.2. In this mode, the PSDA can be switched between two states according to task requirements: the compliant state and rigid state. The PSDA is compliant when the damping orifice is open, as shown in Fig.8 (b), and the dynamic model of PSDA is

$$\begin{cases} \tau_m - D_t(\Delta x_0)(\dot{\theta}-\dot{q})^2 \operatorname{sgn}(\dot{\theta}-\dot{q}) - D_m\dot{\theta} - K(\theta - q) = J_m\ddot{\theta} \\ D_t(\Delta x_0)(\dot{\theta}-\dot{q})^2 \operatorname{sgn}(\dot{\theta}-\dot{q}) + K(\theta - q) - D_l q = J_l\ddot{q} \end{cases} \tag{14}$$

where q and $\dot{q}$ are the position and velocity of the output link respectively. In the rigid state, as shown in Fig.8 (c), the orifice will be completely closed to eliminate the relative movement between the input and output links, so the dynamic model can be described as

$$\tau_m - (D_m + D_l)\dot{q} = (J_m + J_l)\ddot{q} \tag{15}$$

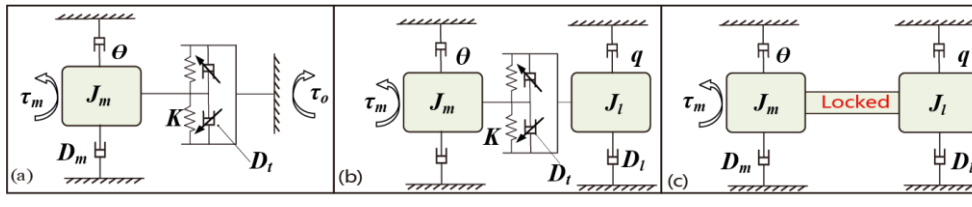

Figure 8. *Model of the PSDA: (a) force control, (b) position control in compliant state, (c) position control in rigid state.*

5. Control Algorithm and Simulation

In this section we first proposed a variable damping algorithm to control the damping of the PSDA, then we proposed the force and position control schemes that both incorporate the variable damping algorithm.

5.1. Variable Damping Control

The aim of variable damping control is to set the damping coefficient D_t to a desired value. According to Eq. (11), the damping coefficient D_t can be considered as a function of the effective area A_0, which is determined by the flap displacement Δx1. Note that, the flap displacement Δx1 is actually controlled by the displacement of the linear motor M2, Δx_o. The relationship between Δx_0 and Δx_1, can be written as

$$\pi\left(\frac{D}{2}\right)^2 \Delta x_0 = 2\pi\left(\frac{d}{2}\right)^2 \Delta x_1 \tag{16}$$

By combining (11) with (16), the displacement of the linear motor $\triangle x_0$ with respect to a desired damping value D_{t_d} can be obtained as

$$\triangle x_0 = 2\sqrt{\frac{h^2(R^2-r^2)^2\rho}{2C_q{}^2 D_{t\_\mathrm{d}}}}\frac{d^2}{D^2 y} \tag{17}$$

Theoretically, we can obtain the desired damping by achieving this motor displacement $\triangle x_0$. However, the accurate identification of those parameters in Eq. (17) is difficult, especially for the flow coefficient C_q, which may vary slightly due to wear situation and the viscosity of the hydraulic oil. To compensate for these errors, a feedback loop is implemented by using an estimated damping coefficient from the measurable states of the system. The estimation is based on the dynamic equation on the motor side

$$D_{t\_e} = \frac{\tau_m - J_m\ddot{\theta} - K\theta}{\dot{\theta}^2} \tag{18}$$

The sum of spring and damping torques, denoted as $\tau_s = \tau_m - J_m\ddot{\theta}$, can be measured with a torque sensor mounted on the PSDA output link, while the angular positions θ and q are measured with the encoders. The angular velocity is obtained by numerical derivative of the position data. The estimated damping coefficient is therefore

$$D_{t\_e} = \frac{\tau_s - K\theta}{\dot{\theta}^2} \tag{19}$$

The damping control algorithm is shown in Fig.9, where Eq. (17) and (19) are implemented in the "Elongation Computation" and "D_t Estimator", respectively.

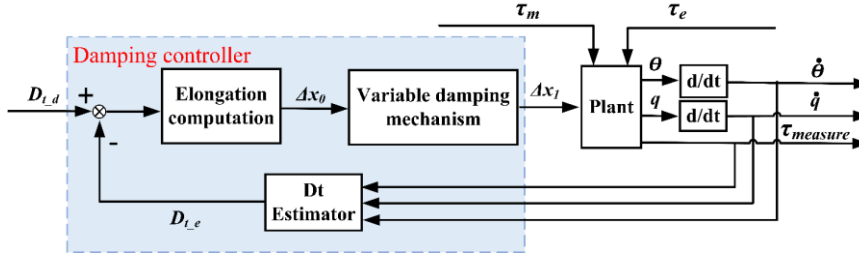

Figure 9. *The variable damping control scheme*

By means of the damping controller proposed in the Fig.9, we can regulate the damping coefficient of the PSDA to a desired value. The next question is how to determine the desired value, i.e., how to obtain the appropriate variable damping strategy in force control and position control.

Bicchi et al. proposed a variable stiffness strategy in [38] that can improve the dynamic performance and ensure safety of the system. It increases the stiffness at the start and stop phases of the motion trajectory where the fast response is the priority. However, it reduces the stiffness during the steady state periods of the motion to ensure sufficient compliance. This strategy inspires our work on the control of the PSDA. The system needs a good dynamic response when the desired force or position signal changes rapidly. This can be achieved by increasing the damping as mentioned in Section 2. The application of this variable damping strategy to force control and position control will be described in section 5.2 and section 5.3, respectively.

5.2. Force Control

The purpose of force control is to make the PSDA an ideal force source which is able to track the

desired force signal with high bandwidth. This is important for higher-order force control [28], such as operational space control, virtual model control and impedance control. At the same time, we also need to guarantee the compliance of the actuator. To meet the above requirements, we use the derivative of the desired torque to determine the damping level as follows

$$D_{t\_d} = D_a + K_1 \left|(1 + d(\tau_d)/dt)\right| \tag{20}$$

where D_a is the initial damping of the system (i.e., the damping when the orifice is completely open), K_1 is a differential coefficient and $d(\tau_d)/dt$ is the derivative of the desired torque signal τ_d with respect to time. Equation (20) can reflect the trend of the input signal, which means it can increase the damping when the desired force signal changes rapidly or reduce the damping when the reference signal gets smooth.

Equation (20) has been implemented in the force control scheme, denoted as "D_t generator" in Fig.10, to provide the desired damping D_{t_d}. The damping controller proposed in Fig.9 is used in the force control scheme as the "D_t controller". The "D_t generator" and the "D_t controller" form a damping regulator that is cooperated with the classic force control loop using a standard PID controller.

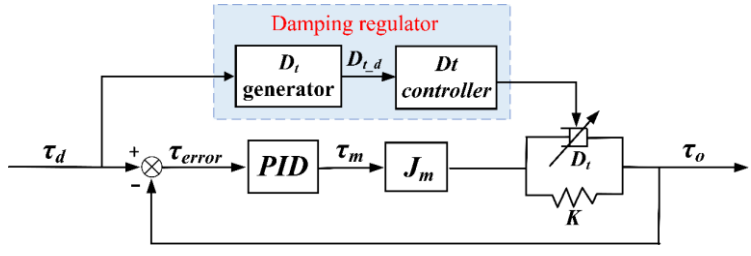

Figure 10. *Output force control scheme*

Two simulations were performed to verify the performance of the proposed force control scheme. The values of the simulated parameters were shown in Table II. Firstly, we used a step signal as the desired torque to see the effect of the damping regulator.

We set the differential coefficient K_1 = 0,0.01,0.05,0.1. As shown in Fig.11, if K_1 was set to 0, the PSDA is equivalent to an SEA and cannot output stable and reliable torque with a PID controller. The output torque of the actuator has serious oscillations. However, with the increase of the K_1, the output torque can gradually get stable with the same PID controller, and the response speed is improved. When K_1 >0.01, the oscillation of output torque can be completely suppressed, and the output response time can also be improved to 0.01S. When K_1 > 0.05, the further increase of K_1 does not improve the output force response significantly. Thus, the appropriate range for K_1 is 0.01 to 0.05.

TABLE II

Identified Parameters of the PSDA Prototype

Parameter	Description	Value
J_m	motor side inertia	0.0532 kg/m2
J_l	Link side inertia	0.0142 kg/m2
K	Spring stiffness	12.34 Nm/rad
D_a	Initial damping	0.05 Nms/rad^2

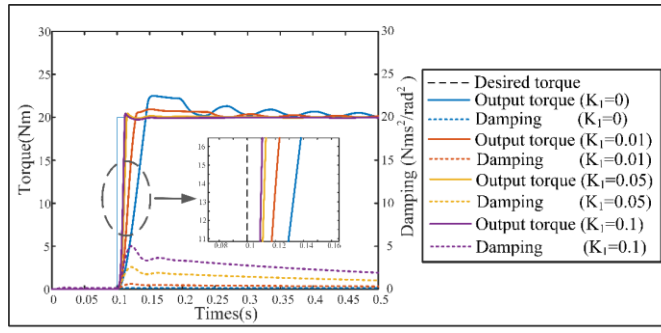

Figure 11. *Step torque output response. By increasing the value of the differential coefficient K_1, the output torque gets stable gradually. The response gets fast due to the rise in damping, and the damping decreases after the output torque is stabilized.*

In the second test, we evaluated the ability of the PSDA to track a square-wave torque signal. From Fig. 12(a), we can see that the output torque has considerable oscillations at the edge of the desired square signal if a pure PID controller is used. With the help of the damping regulator, we can predict the change of the desired torque signal and tune the damping in real time to suppress the oscillation, as shown in Fig.12(b). The damping will increase when the desired torque signal change rapidly yet decreases when the change is stable. The energy consumption in this process can be obtained by integrating the control signal motor torque τ_m. It can be seen in Fig. 12(c) that the system with damping regulator consumes only a quarter of the energy in comparison to the one without damping regulator. Based on the above simulated results, compared with SEA, the PSDA can generate more stable and rapid output torque while saving energy.

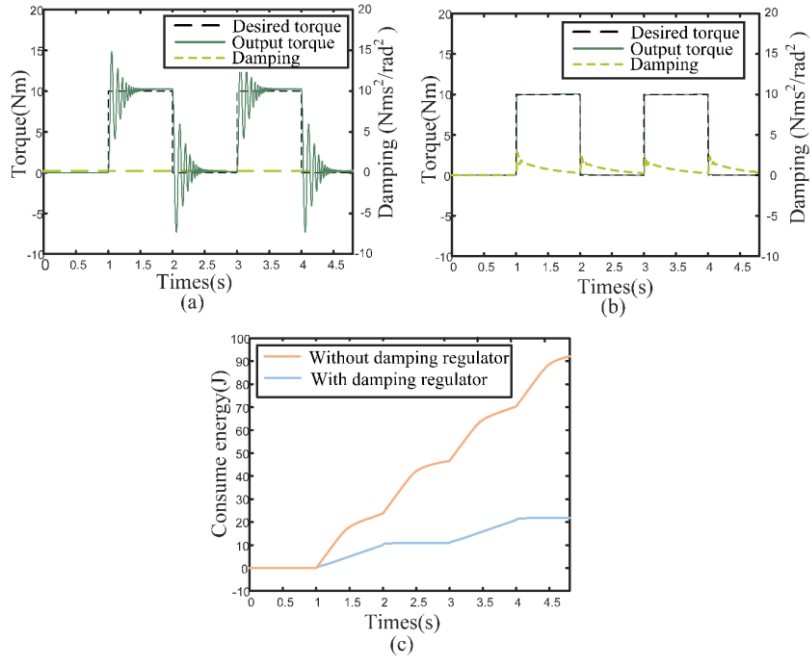

Figure 12 *Force control under Square-wave torque signal: (a) Without the damping regulator, the damping signal is kept at a low level and the output oscillates when the desired signal changes. (b)*

With the damping regulator, the damping signal rises when the desired signal changes drastically, the oscillations of the output are suppressed, and the damping signal gradually falls when the output is smooth. (c) the comparison of consumed energy.

5.3. Position Control

For the position control, we also used the variable damping strategy mentioned in Section 5.1. Similar to the force control, the derivative of the desired position signal is used to determine the damping as

$$D_{t\_d} = D_a + K_q \left| (1 + d(q_d)/dt) \right| \tag{21}$$

where $d(q_d)/dt$ is the derivative of the desired position signal q_d with respect to time, and $K_q$is the differential coefficient. Equation (21) has been implemented in the position control scheme, denoted as "D_t generator" in Fig.12, to provide the desired damping D_{t_d}. The damping controller proposed in Fig.9 is used in the "D_t controller". The "D_t generator" and the "D_t controller" form a damping regulator, and a standard PID controller is used in the closed control loop.

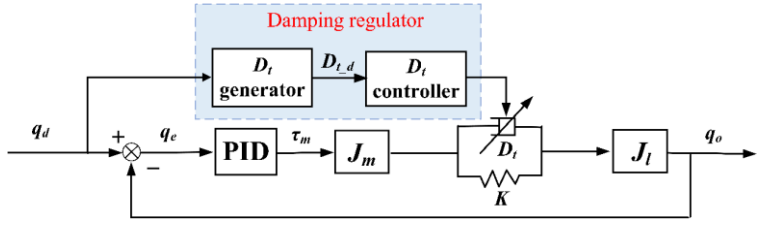

Figure 13*. Output position control scheme*

We also performed a simulation to verify the performance of the proposed control scheme. Without the damping regulator (K_q is set to 0), it can be seen in Fig. 14 that the position step response of the PSDA does not oscillate when the proportional coefficient of the PID controller P is low, P<2, but with a response time of more than 1s. The response time can be reduced by increasing the gain of the PID controller, but this resulted in oscillations in the system. Finally, we allowed the response time to be reduced to 0.3s by adjusting the PID control parameters appropriately (P=5 I=15 D=8). However, with the help of the damping regulator we proposed, the response time can be further reduced to 0.2s without system oscillation.

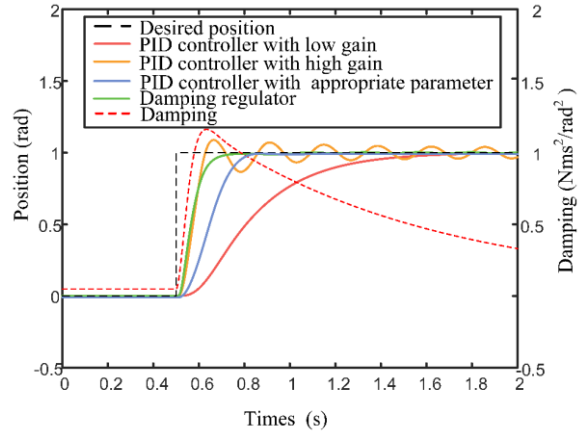

Figure 14. *Step response of the position control. Without adjusting the damping, the system may experience longer response time and oscillations. Altering the PID control parameters can slightly*

mitigate the response time issue. However, implementing the damping control regulator proposed in this study can result in a significantly faster response time of 0.2 second, while also eliminating oscillations.

6. Experiment

Four experiments were carried out to test the performance of the PSDA. The experimental setup is shown in Fig.15(a). The laptop is used as a host computer to run the control algorithms presented in Section 5. The motion controller (Model type: JMC101, produced by JieMeikang) receives the commands from the host computer and perform real-time servo control for the torque motor M1 (Model type: KAH-17A, produced by KaiserDrive) and linear motor M2 (Model type:LA10, produced by InspireRobot). The motor M1 requires an external servo driver (Model type: CDHD2-0151DAF1, produced by ServoTronix) to amplify the current, whereas the M2 has an integrated driver inside.

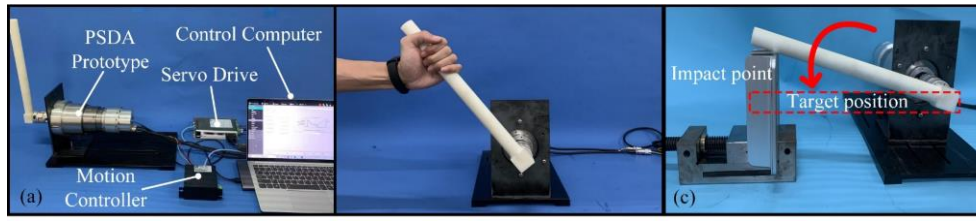

Figure 15. *PSDA Experiments (a) the experiment setup, (b) damping experiment (c) impact experiment*

6.1. Variable Damping Control Experiment

This experiment was to verify the variable damping capacity of the damper. The elastic element (spring) was removed and the PSDA is therefore used as a series-damper-actuator (SDA). The output link of the PSDA was subjected to external force resulting in different velocities, see Fig. 15(b). The torque sensor and encoder recorded the damping torque at different velocities.

The damping was set from 0.5 to 5 Nms^2/rad^2. Fig.16 shows the torque-velocity plot by applying clockwise/counterclockwise torque for 3 tests respectively, and 40 sampled points were recorded in each of them. It can be seen that the sampled points of torque and velocity are basically located near the theoretical curve obtained from Eq. (10), and the direction of the torque is opposite to the velocity. The errors are mostly due to the liquid leakage, which are increasing as the applied torque getting larger.

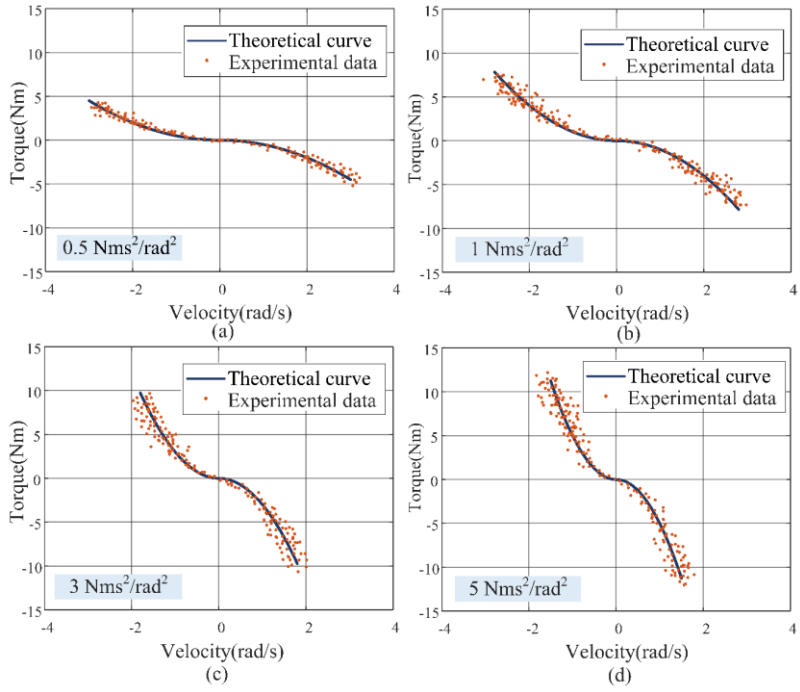

***Figure 16**. Experimental data at different damping levels (a) D_t = 0.5 Nms^2/rad^2, (b) D_t = 1 Nms^2/rad^2, (c) D_t =3 Nms^2/rad^2 and (d) D_t = 5 Nms^2/rad^2. The sampled points of torque and velocity are basically located near the theoretical curve obtained from Eq. (10), and the direction of the torque is opposite to the velocity.*

6.2. Impact experiment

In this experiment we use a complete PSDA prototype to test the effect of damping on the compliance of the system. We presented the torque data near the impact torque to provide a clear illustration of the torque response under different damping conditions (D_t=0.1, 0.5, 1, 5). For a specific damping condition, the impact test was repeated 3 times with a sampling rate of 400Hz. We plot the average values of the torque data obtained from the 3 tests. As shown in Fig.15(c), the output link of the PSDA hit an obstacle during the rotating movement with an initial velocity of 0.5 rad/s, and the impact torque acting on the PSDA was shown in Fig.17. The rise of the impact torque becomes sharp as the damping increases. The rise time for the impact torque to reach its peak is about 0.01s when the damping is set to 10 Nms^2/rad^2, but increases to 0.1s at low damping condition. This is why we set the system to a low damping condition in the control algorithms proposed in Eq. (20) and (21), making the system have better compliance and more time to absorb the impact. We only increase the damping when the system needs to respond quickly to the reference signal.

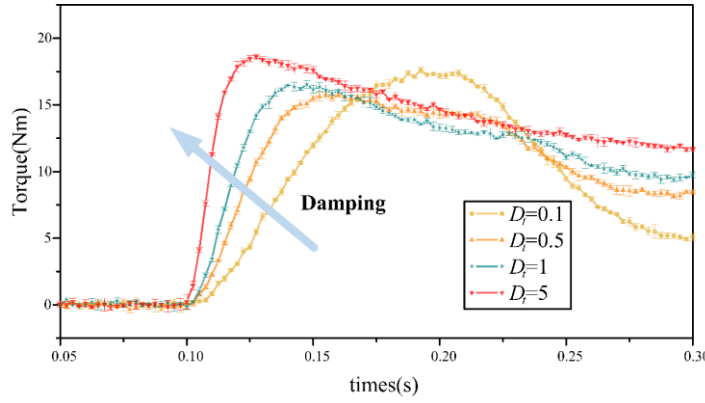

Figure 17. *Experimental data for impact tests.* The rise of the impact torque becomes sharp as the damping increases. The rise time for the impact torque to reach its peak is about 0.01s when the damping is set to 10 Nms^2/rad^2, but increases to 0.1s at a low damping condition.

6.3. Force Control Experiments

The purpose of this experiment is to test the force control performance of the PSDA. The output torque is collected by the torque sensor mounted on the output link. The damping can be estimated according to Eq. (19).

As shown in Fig.18, we run a set of torque response tests with step input. Firstly, we open the damping orifices completely by setting the displacement of flap $\triangle x_1 = 0$. This means that we disabled the damping regulator presented in Fig.10. Thus, the damping is kept at a low level near zero, and the output torque has obvious oscillations when the desired torque signal changes drastically. However, with the help of damping regulator, the damping rises rapidly to 4.2 Nms^2/rad^2 when the desired signal changes. We conducted 5 repeated tests, resulting in a 75% suppression of overshoot on average. The oscillations of the output torque are well suppressed, and the response time is reduced considerably, from 0.04s to 0.01s.

We also utilized square wave as the reference input to further test the ability to track force trajectories in a long-term process. As shown in Fig.19, although the outputs in both tests can follow the reference with a period of 2 s. It can be seen that a lot of oscillations in the torque output if the damping regulator is disabled, Fig.19(a). On the other hand, the damping regulator can increase the damping level to 4.2 Nms^2/rad^2 at the edge of the square wave while reduce it to 0.6 Nms^2/rad^2 at the flat part of the square wave, Fig.19(b). The variable damping strategy significantly suppress the oscillations in torque control.

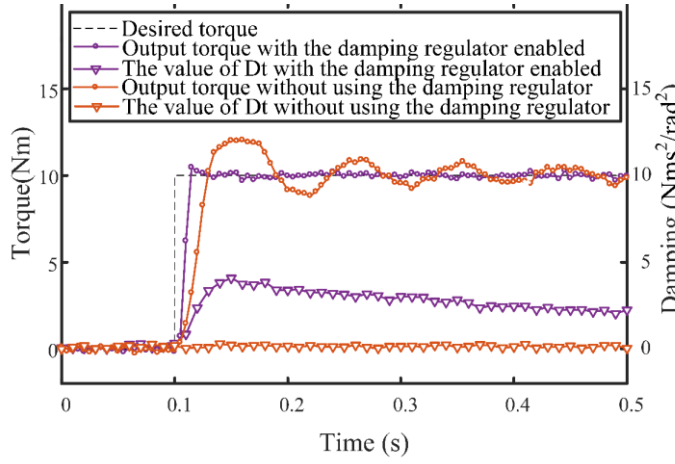

Figure 18. *Experimental data for torque control with step input. When damping is maintained at a minimal level close to zero, a rapid change in the desired torque signal will cause significant oscillations in the output torque. However, using the damping regulator, damping rapidly increases to* 4.2 Nms^2/rad^2 *as the desired signal changes, then decreases as the output gets smooth. As a result, oscillations in the output torque are effectively suppressed, and the response time is significantly reduced from* 0.04 *to* 0.01 *second.*

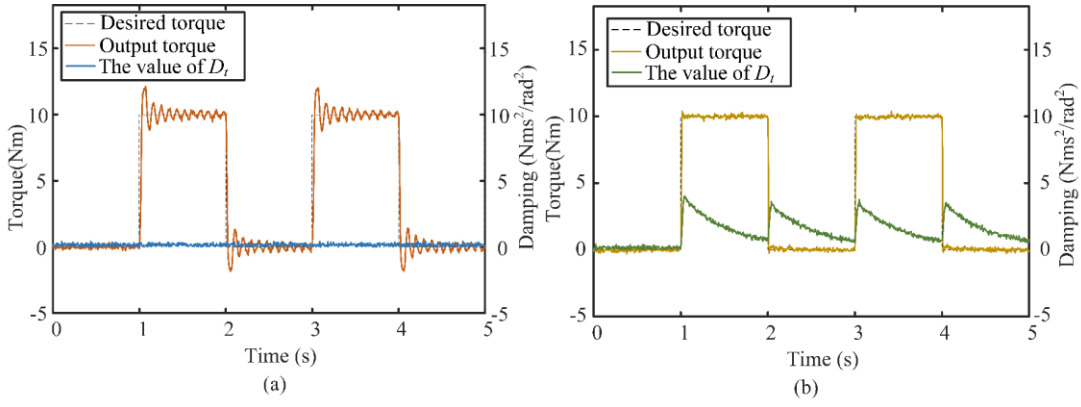

Figure 19. *Experimental data for torque control with square wave signal (a) With the damping regulator disabled, the damping is kept at a low level and the output oscillates when the desired signal changes. (b) With the damping regulator enabled, the damping rises when the desired signal changes drastically, the oscillations of the output are suppressed, and the damping gradually falls when the output is stable.*

6.4. Position Control Experiments

This experiment validated the performance of the PSDA in position control. The output position q is collected by the encoder mounted on the output link. The damping can be estimated according to Eq. (18).

Four step response tests were carried out. Firstly, we set the damping orifices to be fully open all the time to disable the damping regulator. As shown in Fig. 20(a), the damping is kept at a low level

near zero and the oscillates occurs until 1.5s. After using the damping regulator, the damping can rise to 0.5 Nms2/rad2 when the step comes. As a result, not only the oscillation was suppressed, but the response time was also reduced to within 0.3s. We conducted 5 repeated tests, resulting in an average reduction of 50% in the response time of the output position.

In our design, the PSDA has the ability to switch from compliant state to rigid state by completely closing the damping orifice. Therefore, the PSDA can be used as a rigid actuator to further improve the position control performance. We conducted 5 tests, and presented the average values of these 5 tests in Fig.20(b). It can be seen that a reduction of 35% in the response time of the output position is achieved by switching the state from compliant to rigid.

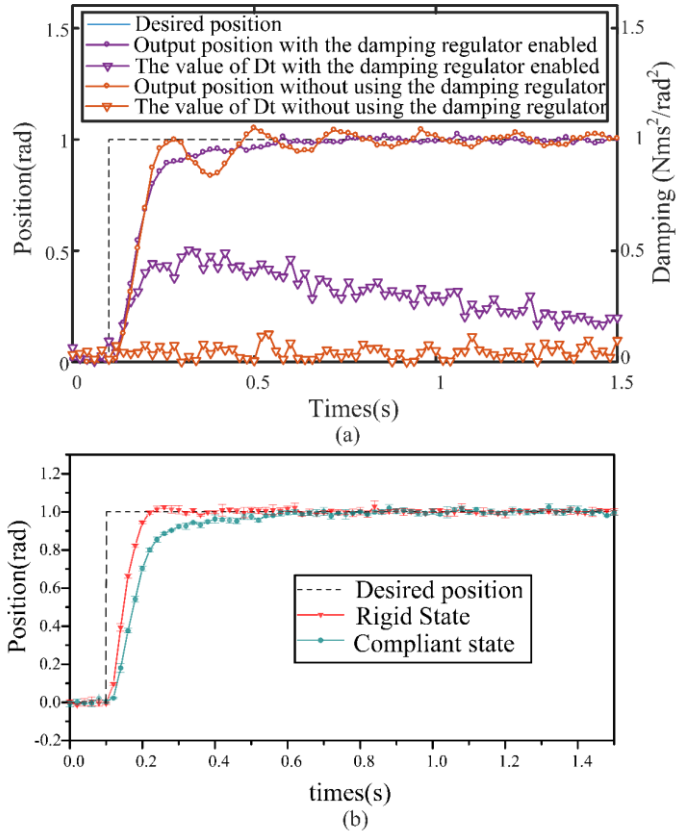

Figure 20. *Experimental data position control with step input (a) effect of the variable damping. Without damping regulator, the damping remains low near zero and the position output oscillates, but with the regulator, the damping rises to* 0.5 Nms^2/rad^2 *as the step arrives and then falls as the output gets stable. Not only are oscillations suppressed, but the response time is reduced to less than* 0.3s. *(b) Comparison of rigid and compliant state in position control. The rigid state reduces the response time from* 0.3 *second to* 0.2 *second compared to the compliant state with damping regulator.*

6.5. discussion

The experimental results demonstrated that the PSDA has a good variable damping capability. From Fig.16, it can be seen that the actual torque-velocity points aligned closely with the theoretical curve.

While some discrepancies can be attributed to internal leakage of the hydraulic oil. It was found that the error increases with the applied torque. This could be due to the fact that the internal pressure of the damper increases as the applied torque increases, leading to more leakage. In view of the experimental results of variable damping force and position control shown in Fig. 18, 19, and 20, such errors can be ignored and the effect of variable damping is satisfactory.

It has been well known that compliant actuators, like SEA, present challenges in dynamic control when compared to their rigid counterparts. More complex and advanced control algorithms are therefore needed for compliant actuators to achieve control compensation. Previous works have employed adaptive neural networks to control SEAs, and achieved excellent results in trajectory tracking [8, 39]. In contrast, our actuator employs a variable damping strategy that directly addresses the dynamic limitations and reduces control complexity. By adjusting physical damping, we achieved satisfactory positioning and force control with a simple PID control method. Additionally, our actuator is able to switch between the compliant and rigid states based on task requirements, enabling it to handle situations that SEAs cannot manage.

In comparison to existing variable damping actuators based on friction[26], magnetorheological, and electrorheological principles[34-36], the PSDA proposed in this paper utilizes orifice effect to achieve damping adjustment, avoiding the continuous consumption of energy to maintain damping. While there were variable damping actuators using orifice effect[40], our PSDA embeds the variable damping mechanism within the rotating shaft of the actuator, making it more compact and suitable for robotic applications. Unlike previous control strategies that directly increased damping to suppress oscillations, the variable damping algorithm proposed in this paper predicts the trend of the reference signal and increases damping only when the reference signal changes drastically. This ensures the compliance of the actuator during smooth movement while suppressing the oscillations and improving the bandwidth when fast response is required.

However, the PSDA has its limitations. The principle of variable damping in PSDA is based on the orifice effect, and achieved by a hydraulic transmission mechanism described in Fig.7. This mechanism may introduce leaking issues. This explains the deviation of the experimental data in the variable damping control experiment, as shown Fig. 16. Furthermore, the damping feedback in this study employs the estimated value calculated from the output position and torque, according to Eq. (19). This process may include noise from the measurement and the differential calculation, which affects the accuracy of feedback. We will improve the design of the actuator to reduce the probability of leaking, and employ state estimators, such as Kalman filtering, to reduce the influence of noise. Besides, our experiments were mostly carried out in short-term. The reliability of the actuator in long-term applications needs to be verified in the future.

7. Conclusion

In this paper, a novel physically compliant actuator, parallel spring-damping actuator (PSDA), is presented, whose transmission mechanism is composed of an elastic element and a variable damper arranged in parallel. The variable damping is achieved by adjusting the effective area of the fluid orifices. This design allows for the regulation and maintenance of the physical damping without large energy consumption. Moreover, the PSDA can be used as a rigid actuator by completely closing the fluid orifice if necessary. The dynamic model of the PSDA were investigated with respect to different control modes. Following this, the variable damping strategy and corresponding force/position control schemes are presented. The simulated and experimental results show that the proposed PSDA can effectively suppress the oscillations and improve the dynamic response of the system.

Required Declarations

Author contributions. Rongjie Kang and Peikang Yuan conceived and designed the study. Jianbin Liu, Zhibin Song and Shuai Wu conducted data gathering. David T Branson performed statistical analyses. Peikang Yuan, Rongjie Kang and Jian S. Dai wrote the article.

Financial support. This work was supported by the National Natural Science Foundation of China under Grant No.: 52375023 and 51975401.

Conflicts of interest. The authors declare no conflicts of interest exist.

Ethical approval. Not applicable.

References

[1] H.-S. Kim, I.-M. Kim, C.-N. Cho, and J.-B. Song, Safe Joint Module for Safe Robot Arm Based on Passive and Active Compliance Method, Mechatronics 22(7), 1023-1030 (2012).
[2] T. Boaventura, J. Buchli, C. Semini, and D. G. Caldwell, Model-Based Hydraulic Impedance Control for Dynamic Robots, *IEEE Trans. Robot.* **31**(6), 1324-1336 (2015).
[3] B. Vanderborght *et al.*, Variable Impedance Actuators: A Review, *Robot. Auton. Syst.* **61**(12), 1601-1614 (2013).
[4] R. V. Ham, T. G. Sugar, B. Vanderborght, K. W. Hollander, and D. Lefeber, Compliant Actuator Designs, *IEEE Robot. Autom. Mag.* **16**(3), 81-94 (2009).
[5] A. Ghafoor, J. S. Dai, and J. Duffy, Stiffness Modeling of the Soft-Finger Contact in Robotic Grasping, *Journal of Mechanical Design* **126**(4), 646-656 (2004).
[6] H. Dong, E. Asadi, C. Qiu, J. Dai, and I. M. Chen, Geometric Design Optimization of an under-Actuated Tendon-Driven Robotic Gripper, *Robot. Comput.-Integr. Manuf.* **50**(80-89 (2018).
[7] G. A. Pratt and M. M. Williamson. Series Elastic Actuators. **In:***Proceedings 1995 IEEE/RSJ International Conference on Intelligent Robots and Systems. Human Robot Interaction and Cooperative Robots*, (1995) pp. 399-406
[8] X. Ren, Z. Li, M. Zhou, and Y. Hu, Human Intention-Aware Motion Planning and Adaptive Fuzzy Control for a Collaborative Robot with Flexible Joints, *IEEE Transactions on Fuzzy Systems* **31**(7), 2375-2388 (2023).
[9] A. Calanca and P. Fiorini, Human-Adaptive Control of Series Elastic Actuators, *Robotica* **32**(8), 1301-1316 (2014).
[10] W. Ju, R. Kang, B. Li, Z. Song, and S. Zhang, Design of a Torsional Compliant Mechanism with Given Discrete Torque-Deflection Points for Nonlinear Stiffness Elastic Actuator, *Robotica* **41**(9), 2571-2587 (2023).
[11] S. Oh and K. Kong, High-Precision Robust Force Control of a Series Elastic Actuator, *IEEE-ASME Trans. Mechatron.* **22**(1), 71-80 (2017).
[12] E. A. B. Nieto, S. Rezazadeh, and R. D. Gregg, Minimizing Energy Consumption and Peak Power of Series Elastic Actuators: A Convex Optimization Framework for Elastic Element Design, *IEEE-ASME Trans. Mechatron.* **24**(3), 1334-1345 (2019).
[13] A. Calanca and T. Verstraten, An Energy Efficiency Index for Elastic Actuators During Resonant Motion, *Robotica* **40**(5), 1450-1474 (2022).
[14] J. Sun, Z. Guo, D. Sun, S. He, and X. Xiao, Design, Modeling and Control of a Novel Compact, Energy-Efficient, and Rotational Serial Variable Stiffness Actuator (Svsa-Ii), *Mech. Mach. Theory* **130**(123-136 (2018).
[15] J. B. Morrell and J. K. Salisbury. Parallel Coupled Actuators for High Performance Force Control: A Micro-Macro Concept. **In:***Proceedings 1995 IEEE/RSJ International Conference on Intelligent Robots and Systems. Human Robot Interaction and Cooperative Robots*, (1995) pp. 391-398 vol.1
[16] M. Zinn, O. Khatib, B. Roth, and J. K. Salisbury, Playing It Safe [Human-Friendly Robots], *IEEE Robot. Autom. Mag.* **11**(2), 12-21 (2004).
[17] S. Wolf *et al.*, Variable Stiffness Actuators: Review on Design and Components, *IEEE-ASME Trans. Mechatron.* **21**(5), 2418-2430 (2016).
[18] Y. Xu, K. Guo, J. Sun, and J. Li, Design, Modeling and Control of a Reconfigurable Variable Stiffness Actuator, *Mech. Syst. Signal Proc.* **160**(107883 (2021).
[19] P. Bilancia, G. Berselli, and G. Palli, Virtual and Physical Prototyping of a Beam-Based Variable Stiffness Actuator for Safe Human-Machine Interaction, *Robot. Comput.-Integr. Manuf.* **65**(101886 (2020).
[20] X. Fu, Y. Li, W. Wang, and C. Yun, Design and Implementation of a Variable Stiffness Actuator Based on Flexible

Gear Rack Mechanism, *Robotica* **36**(3), 448-462 (2018).
[21] M. Harder, M. Keppler, X. Meng, C. Ott, H. Höppner, and A. Dietrich, Simultaneous Motion Tracking and Joint Stiffness Control of Bidirectional Antagonistic Variable-Stiffness Actuators, *IEEE Robotics and Automation Letters* **7**(3), 6614-6621 (2022).
[22] R. Mengacci, M. Garabini, G. Grioli, M. G. Catalano, and A. Bicchi, Overcoming the Torque/Stiffness Range Tradeoff in Antagonistic Variable Stiffness Actuators, *IEEE-ASME Trans. Mechatron.* **26**(6), 3186-3197 (2021).
[23] Y. Liu, X. Liu, Z. Yuan, and J. Liu, Design and Analysis of Spring Parallel Variable Stiffness Actuator Based on Antagonistic Principle, *Mech. Mach. Theory* **140**(44-58 (2019).
[24] J. Hurst, A. Rizzi, and D. Hobbelen. Series Elastic Actuation: Potential and Pitfalls. **In:***International conference on climbing and walking robots*, (2004) pp.
[25] S. Monteleone, F. Negrello, M. G. Catalano, M. Garabini, and G. Grioli, Damping in Compliant Actuation: A Review, *IEEE Robot. Autom. Mag.* **29**(3), 47-66 (2022).
[26] M. Laffranchi, N. G. Tsagarakis, and D. G. Caldwell, Analysis and Development of a Semiactive Damper for Compliant Actuation Systems, *IEEE-ASME Trans. Mechatron.* **18**(2), 744-753 (2013).
[27] C.-M. Chew, G.-S. Hong, and W. Zhou, Design of Series Damper Actuator, *Robotica* **27**(3), 379-387 (2009).
[28] N. Paine, S. Oh, and L. Sentis, Design and Control Considerations for High-Performance Series Elastic Actuators, *IEEE-ASME Trans. Mechatron.* **19**(3), 1080-1091 (2014).
[29] H. Vallery, J. Veneman, E. v. Asseldonk, R. Ekkelenkamp, M. Buss, and H. v. D. Kooij, Compliant Actuation of Rehabilitation Robots, *IEEE Robot. Autom. Mag.* **15**(3), 60-69 (2008).
[30] N. L. Tagliamonte and D. Accoto, Passivity Constraints for the Impedance Control of Series Elastic Actuators, *Proc. Inst. Mech. Eng. Part I-J Syst Control Eng.* **228**(3), 138-153 (2013).
[31] N. S. Nise, *Control Systems Engineering*. John Wiley & Sons, 2020.
[32] M. Laffranchi, N. G. Tsagarakis, and D. G. Caldwell. A Variable Physical Damping Actuator (Vpda) for Compliant Robotic Joints. **In:***IEEE International Conference on Robotics and Automation*, (2010) pp. 1668-1674
[33] J. Sun, Z. Guo, Y. Zhang, X. Xiao, and J. Tan, A Novel Design of Serial Variable Stiffness Actuator Based on an Archimedean Spiral Relocation Mechanism, *IEEE-ASME Trans. Mechatron.* **23**(5), 2121-2131 (2018).
[34] J.-S. Oh, J. W. Sohn, and S.-B. Choi, "Applications of Magnetorheological Fluid Actuator to Multi-Dof Systems: State-of-the-Art from 2015 to 2021," *Actuators*, vol. 11, no. 2. doi: 10.3390/act11020044
[35] G. Ramkumar *et al.*, Synthesis Characterization and Functional Analysis of Magneto Rheological Fluid – a Critical Review, *Materials Today: Proceedings* **66**(760-774 (2022).
[36] Z. Ullah, R. Chaichaowarat, and W. Wannasuphoprasit, "Variable Damping Actuator Using an Electromagnetic Brake for Impedance Modulation in Physical Human&Ndash;Robot Interaction," *Robotics*, vol. 12, no. 3. doi: 10.3390/robotics12030080
[37] N. G. Tsagarakis, M. Laffranchi, B. Vanderborght, and D. G. Caldwell. A Compact Soft Actuator Unit for Small Scale Human Friendly Robots. **In:***IEEE International Conference on Robotics and Automation*, (2009) pp. 4356-4362
[38] A. Bicchi, G. Tonietti, M. Bavaro, and M. Piccigallo. Variable Stiffness Actuators for Fast and Safe Motion Control. **In:***Robotics Research. The Eleventh International Symposium*, (2005) pp. 527-536
[39] X. Ren, Y. Liu, Y. Hu, and Z. Li, Integrated Task Sensing and Whole Body Control for Mobile Manipulation with Series Elastic Actuators, *IEEE Transactions on Automation Science and Engineering* **20**(1), 413-424 (2023).
[40] D. Zhi, Z. Feng, W. Xu, R. Kang, and L. Chen. Design and Control of a Variable Viscous Damping Actuator (Vvda) for Compliant Robotic Joints. **In:***2018 IEEE International Conference on Robotics and Biomimetics (ROBIO)*, (2018) pp. 1876-1881